Identification and Control of a River-Current-Turbine Generator-Application to a Full-Scale Prototype

Matthieu Hauck, Axel Rumeau, Antoneta Iuliana Bratcu, Seddik Bacha, Iulian Munteanu, Daniel Roye

▶ **To cite this version:**

Matthieu Hauck, Axel Rumeau, Antoneta Iuliana Bratcu, Seddik Bacha, Iulian Munteanu, et al.. Identification and Control of a River-Current-Turbine Generator-Application to a Full-Scale Prototype. IEEE Transactions on Sustainable Energy , 2018, 9 (3), pp.1365-1374. 10.1109/TSTE.2017.2782759 . hal-01659739

HAL Id: hal-01659739
https://hal.science/hal-01659739

Submitted on 17 Dec 2017

HAL is a multi-disciplinary open access archive for the deposit and dissemination of scientific research documents, whether they are published or not. The documents may come from teaching and research institutions in France or abroad, or from public or private research centers.

L'archive ouverte pluridisciplinaire **HAL**, est destinée au dépôt et à la diffusion de documents scientifiques de niveau recherche, publiés ou non, émanant des établissements d'enseignement et de recherche français ou étrangers, des laboratoires publics ou privés.

Identification and control of a river-current-turbine generator – application to a full-scale prototype

Matthieu Hauck, Axel Rumeau, Antoneta Iuliana Bratcu, Seddik Bacha, Iulian Munteanu, Daniel Roye

***Abstract*--This paper reports on the operation assessment of an electrical power generation system based upon cross-flow water turbines. The specific power take-off system has been tested in real-world conditions in a variety of scenarios and the experimental results have confirmed previous modeling assessments. Dynamical proprieties have been precisely identified and stable system operation over the entire operating range has been achieved. Steady-state characterization in terms of power coefficient has also been done, allowing the assessment of power generation system global efficiency and enabling the building of more precise models to be used in further simulations and assessments for power grid integration. Maximum power point tracking and other specific operation regimes such as angular position synchronization have also been validated.**

***Index Terms*--Maximum Power Point Tracking, microhydro power, performance evaluation, power generation control.**

I. Nomenclature

T_T , P_T , Ω_T	turbine torque, power and rotational speed
w , λ , C_p	water flow velocity, turbine tip speed ratio and power coefficient
R_T , H_T	turbine radius and height
J	CFWT-PMSG coupling inertia
D	parameter embedding CFWT's viscous friction and mechanical characteristic slope
Ω_G , T_G	generator rotational speed and torque
K_G , K_Ω	torque and e.m.f. constants
i_{qG} , i_{dG}	*dq* generator currents
$K_{P\Omega}$, $K_{I\Omega}$	rotational speed controller proportional and integral gains

II. Introduction

In recent years renewable energy conversion systems have demonstrated their potential as sustainable alternative to the classical electrical power generation technologies. An intensive research effort has been conducted in order to extend the exploitation range of the free and inexhaustible natural resources. As the marine currents and river flows represent a significant renewable energy potential all around the world, new hydraulic capturing devices that enable harvesting of these resources have been developed in the last years [1], [2], [3]. All these devices harness the water flow energy with minimal environmental impact, involving the use of limited-span civil engineering structures for conditioning the incoming flows. This advantage comes with a drawback consisting in the incompatibility between the irregular, erratic, non controllable and often unpredictable nature of the primary energy resource on a hand, and safety requirements, the load demands (*e.g.*, supposing continuity of service at a given power level) and increasingly restrictive grid codes, on the other hand. However, this situation may be alleviated by means of the power generation control either by using pitchable blades or by controlling the electrical generator at variable speed through the associated power electronics interface. The use of such generators that have quite reduced power ratings, but important territorial spreading is issued from the new paradigm of distributed electrical power generation, recently appeared within the energy market context. Generator control is important in both off-grid mode (stand-alone microgrid) [4] and also in grid-connected applications, for providing ancillary services, such as improving power system stability or damping inter-area oscillations [5], [6].

This work has been partially funded by the National French Agency for Research (Agence Nationale de la Recherche – ANR) in the framework of project HARVEST (*Hydroliennes à Axe de Rotation Vertical Stabilisé*).

M. Hauck, A. Rumeau, S. Bacha and D. Roye are with Grenoble Electrical Engineering Laboratory (G2ELab), Bâtiment GreEn-ER, 21 Avenue des Martyrs, CS 90624, 38031 Grenoble, France (e-mails: matthieu.hauck@gmail.com, axel.rumeau@ac-toulouse.fr, seddik.bacha@g2elab.grenoble-inp.fr).

A. I. Bratcu and I. Munteanu are with Grenoble Image Speech Signal Control Systems Laboratory (GIPSA-Lab), 11 Rue des Mathématiques, 38402 Saint Martin d'Hères, France (e-mails: {antoneta.bratcu, iulian.munteanu}@gipsa-lab.grenoble-inp.fr).

Water-turbine-based generation systems installed in rivers, generally named as microhydro power plants, use various resource capturing devices depending on each particular application. For instance, microhydro power plants use some classical designs such as (semi) Kaplan or Francis water turbines, but the marine-current or river-flow generation systems uses more modern designs such as axial-flow [7], [8], vertical-axis [9], [10] or cross-flow water turbines (CFWT) [11], [12]. Their particular set-up – free-water-flow conditions – invariantly requires the use of modern electrical generator control techniques such as vector control, variable-speed control, maximum power point tracking (MPPT) [2], [8], [13], which may generally be found in renewable power generation technology.

However, as their technology cannot yet be considered mature, these new power generation concepts need proof of concept validation and thoroughly operation assessment, at significant power rating levels. The associated literature offers information about prototypes which are built prior to verify the viability of various hydrodynamic concepts mostly for axial-flow water turbines [14], [15]. CFWT-based prototypes, developed upon variations of Darrieus turbine concept are also present [16]. CFWTs have several advantages *vs*. the axial-flow ones such as smaller cavitation [17], insensitivity to changes of water flow direction, simpler mechanical structure, and more flexible power generation system. With respect to axial turbines, CFWTs present non-negligible drawbacks such as pulsating turbine torque, lower starting torque and lower power coefficient. Recent comprehensive reviews of hydrokinetic turbine technology can be found in [18]–[20].

The work presented in this paper deals with a power generation system prototype built using the Achard turbine developed in [12] that operates in real-world conditions provided by a controlled water stream. Its original hydrodynamic and mechanical design strives to fully use the advantages of CFWT, while minimizing its drawbacks.

Previously-done computer simulation of hydrodynamic behavior and capabilities of the Achard turbine and then tests at reduced scale in laboratory-controlled water stream [21] have predicted the main steady-state and dynamical features of the concerned turbine system. Computer simulations of the turbine-electrical generator coupling and then physical hardware-in-the loop tests have already anticipated variable-speed capabilities and grid-connected operation of the concerned power generation system [21], [22].

This paper reports the demonstration at full scale and operation assessment of a power generation system based upon the Achard CFWT, in real-world conditions, with focus on aspects of electrical power conversion. Main capabilities of a 1:1 prototype have been briefly described in [23]. Basic turbine modeling validation together with turbine system hydro-dynamical characterization and generator control techniques assessment are also targeted. The focus is on electrical power generation and control, while mechanical issues – such as mechanical interaction in between different components, displacement or deformation of the whole structure – are beyond the scope of this paper.

This paper is structured as follows. The next section, the third, describes the CFWT-based power generation system, while Section IV describes the prototype. Section V provides details about the basic operating regimes and their associated control structures. Section VI presents system modeling aspects from the hydro-mechanical point of view. Section VII presents and discusses the experimental results concerning various operation modes. Section VIII concludes the paper.

III. Power Take-off System

The prototype uses a prime mover based upon the three-bladed vertical-axis Achard turbines with straight blades [12], [24] (Fig. 1a). This Achard turbine resulted as an evolution of Darrieus and Gorlov turbines; it has flying-wing-shaped blades fixed on the rotation axis by means of profiled central arms.

A comparative study of Achard, Darrieus and Gorlov turbines has been made in [25]. Thus, results have shown that for a water flow velocity of 2.3 m/s the maximum power point of the three turbines is placed at almost the same value of the tip speed ratio (within 3 to 5% measurement uncertainty), which is $\lambda = 2$. In this configuration, the straight-blade Achard turbine appears to have the best efficiency (33%), followed by Darrieus (31%) and Gorlov (26%) turbines.

In order to achieve better performance and to overcome the drawbacks inherent to vertical axis turbines, a complex power take-off device has been built, as follows. First, four three-bladed CFWTs, have been pilled-up into the same shaft, the obtained structure being called a CFWT tower. In order to smooth the mechanical torque, each turbine has been installed with angular position shifted with $\pi/2$ with respect to the previous one, thus achieving a spatial filtering of the output power, using the same idea as in [22]. In this way one may consider that the turbine power coefficient is almost constant irrespective of the turbine's position with respect to the water flow direction.

A CFWT tower directly drives a permanent synchronous generator, situated in its lower part (Fig. 1b). Generators are thus immerged into water; this solution has been chosen mainly because some cooling system is thus no longer needed. Another choice would be to place generators on tower top, being closer to mainland equipment, thus allowing easier maintenance. Two CFWT towers which rotate in opposite senses are placed side by side into the same structure. Previous analysis has shown that, by using this structure, structural loads may be alleviated in certain operating regimes [24]. Third, the two CFWT towers are encompassed by fairings. This results in increasing the upstream-*vs*.-downstream differential pressure of the CFWT tower, thus allowing increased power capture for certain water conditions.

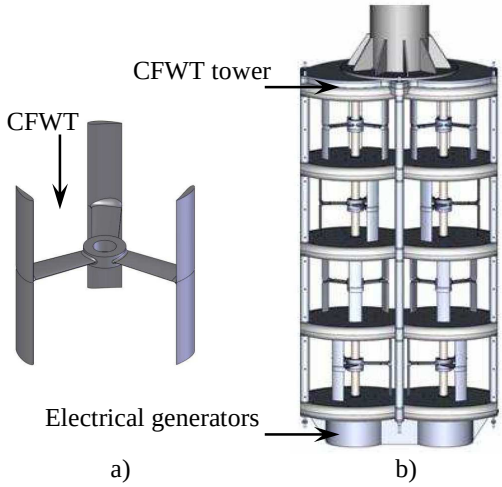

Fig. 1. a) Three-bladed Achard CFWT with straight blades; b) power take-off structure: two adjacent CFWT towers, each with four piled-up turbines [21].

IV. Prototype Description

A. Overall architecture

This section presents the architecture of the generation system with focus on the power capturing device and on electrical power generation subsystem. In order to facilitate turbines testing, the prototype has been installed in a headrace canal feeding a hydroelectric plant. Such choice allowed the anchoring – on riverside or river bed – problem being avoided (Fig. 2a). Also, one can set up the water stream speed by using already existing canal flow control systems.

The supporting frame (left side of Fig. 2) spans over the canal. It has a fastening system which allows rotation and translation motions of turbine assembly – the two CFWT towers – in order to enable easy immersion into water, operation, parking and maintenance. Water velocity is measured by means of a fixed acoustic transducer (Sontek ARGONAUT SW) which uses Doppler effect and is designed to work in slow water flows (between 0.3 m/s and 5 m/s). The channel water velocity is adjusted by using the specific equipment at the downstream hydroelectric power plant.

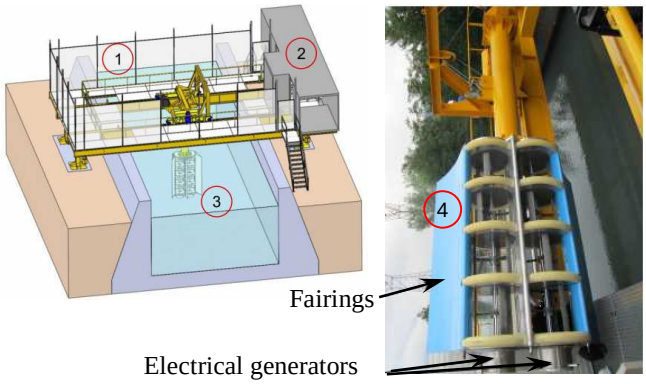

Fig. 2. a) Main components of CFWT-based prototype: 1 – supporting frame, 2 – electrical equipment shelter, 3 – CFWT towers immerged into river canal; b) Details concerning power take-off device: 4 – turbine assembly with turbines piled-up in towers, electrical generators and fairings.

B. Electrical subsystem

The electrical subsystem of a CFWT tower is presented in Fig. 3; it contains a three-phase permanent-magnet synchronous generator (PMSG) coupled directly to the CFWT shaft. This PMSG, specifically customized for the prototype, is characterized by the ability of developing large torque at small rotational speeds. It exhibits constant torque over a wide rotational speed range in order to provide good efficiency irrespective of the operating point [26]. This generator is interfaced with the local power grid by means of an AC-DC-AC power electronics converter which is implemented by using Parvex SSD AC drive [27]. The two CFWT systems corresponding to each Achard CFWT tower within the prototype have the same structure and are connected to the Diesel-generator terminals.

The AC drive contains a three-phase diode rectifier, a DC-link and an inverter (Fig. 3), as being the required configuration for PMSG motoring operation. This however does not prevent the electrical machine operation in generator mode, provided that DC-link power is properly evacuated (*i.e.*, its voltage, v_{DC} , is maintained at a constant value).

The entire prototype operates off-grid, but on-grid operation conditions are emulated so that the system global objectives and

behavior to fit the on-grid operation. Thus, a three-phase Diesel-generator set [28] is used in the start-up phase to energize the DC-link. Once the DC-link is energized, there is no power exchange between the Diesel-generator and the remainder of system, so the generator-rectifier pair behaves like being disconnected from the DC-link.

The DC-link being energized (at a convenient setpoint voltage, v_{DC}^{*}), the power electronics present in the AC drive allows the PMSG being operated at variable speed by means of the classical vector (torque) control [29]. The CFWT operation has been achieved using built-in current and speed control loops of the AC Parker SD drive. The outer control loops have been customized in order to modulate the CFWT behavior accordingly to the water condition and operator decisions.

It is noteworthy that in generation mode the AC drive draws current from the PMSG, thus increasing the DC-link voltage up to the point where diodes from the uncontrolled rectifier become blocked. Therefore, the AC power provided by the Diesel-generator set is used only in the phase of energizing the DC-link. Further, while the system operates in normal conditions, the DC-link voltage is regulated to a constant value by means of a chopper (DC-DC step-down converter) and DC-link in-excess power is evacuated to the dump load (full-power-rated braking resistor in Fig. 3).

Recall that the prototype operates in a remote area, in the absence of power grid. As explained before, this quite complex setup has been conceived such to provide the same environment to the ensemble PMSG-inverter as in the grid-connected case. One can note that this requirement holds as the DC-link voltage is maintained constant (consequence of chopper action) at the rated value. Thus, the CFWT system may be operated at variable speed exactly as in the grid-connected mode, by employing the versatility of torque-controlled PMSG.

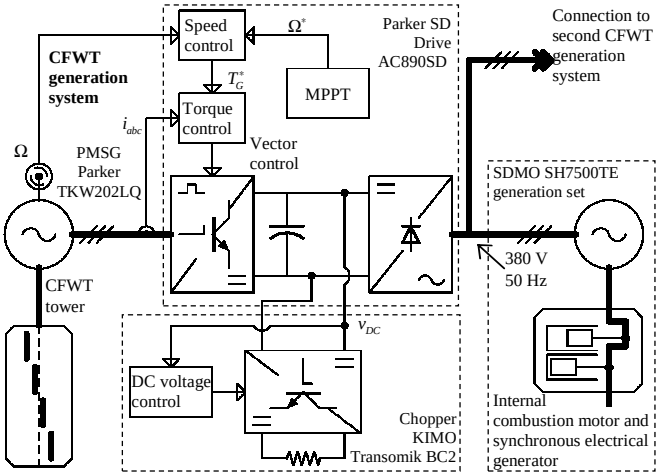

Fig. 3. Diagram of the prototype energy conversion chain for a single CFWT tower.

V. Basic Operation and Associated Control Structures

In this paper focus is on the CFWT tower variable operation, whereas the grid-connection behavior is of less interest. This mainly supposes - at the outermost level - the rotational speed management with respect to the water conditions. Classical cascaded control structure is used in order to achieve the specified goal. This structure is implemented by using the proprietary Parvex SD drive software. The innermost control structure deals with the active and reactive current components control, and is built by using the PMSG *dq* modelling. The rotational speed control is based on feedback from an incremental encoder (as in [22]) and is designed to have significantly slower dynamics than the current control loops.

While the built-in low-level current and rotational speed loops have been modified only by configuring the controllers' parameters, the outer loops that output the rotational speed set point have been entirely built. These various outer loops have different objectives and implement system supervision (start-up, switch between manual, test and automatic modes, etc.), MPPT algorithms and so on. The functionality of these loops may be overviewed in Fig. 3. Finally, it is envisaged that the angular position between the two CFWT towers of prototype be controlled with respect to an imposed criterion that may include reduction of mechanic and hydrodynamic stresses. A fully-functional monitoring system has been implemented into the Parvex software, allowing real-time modification of associated control parameters, operating modes and references through the software interface.

The grid-connection system uses a diode-based (i.e., uncontrolled) grid-side converter – located also in the Parvex SD drive. In order to maintain constant DC-link voltage, the generated electrical power is evacuated from DC link by the DC-DC converter (chopper) into the dump load. DC-link voltage regulation is implemented by a hysteresis control law which drives the chopper switches. Note that, rigorously speaking, this configuration is not representative of an on-grid generation system, as in a genuine grid-connected system – such as within a microgrid – an inverter should normally be present in order to allow power injection into the grid.

VI. Modelling and Rotational Speed Control Aspects

The cross-flow water turbine is derived from the Darrieus turbine ([11], [17]) and has been mainly developed in [12]. The extracted mechanical power depends on the water flow velocity cubed and on the turbine parameters, according to the classical concept of actuator disc operating in free-fluid conditions:

$$P_T = 0.5 \cdot \rho \cdot C_p(\lambda) \cdot S_T \cdot w^3 \qquad (1)$$

where ρ and w are the water density and free-stream water flow velocity respectively, C_p is the power coefficient and S_T is the area of turbine longitudinal section, computed based on the turbine radius, R_T, and the turbine height, H_T, as $S_T = 2R_T \cdot H_T$. The power coefficient is a function of the tip speed ratio, λ, defined as: $\lambda = (R_T \Omega_T)/w$, where Ω_T is the turbine rotational speed. Power coefficient curve – which expresses the turbine energy efficiency – has been assessed in previous works – see for example, [21] – as being unimodal in relation to the turbine's rotational speed for a given water flow velocity. CFWT shaft torque expression is obtained from the extracted power, as

$$T_T = P_T / \Omega_T \, . \qquad (2)$$

Note that the same relations hold for the case of a CFWT tower, provided that tower's power and torque are obtained by summing-up individual turbines' power and torque values, respectively.

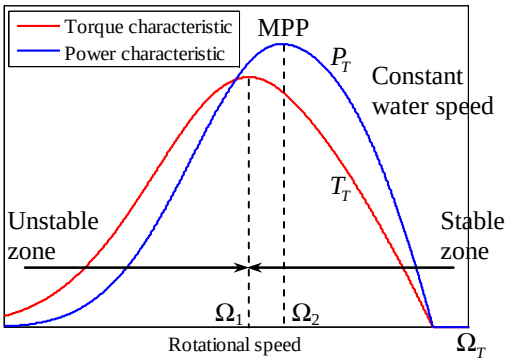

Fig. 4. Torque and power characteristics of a CFWT.

Next, notations refer to a CFWT tower. The PMSG is directly driven by the CFWT tower; the motion equation of their coupling is

$$J \cdot \dot{\Omega}_T = T_T(\Omega_T, w) - f \cdot \Omega_T - T_G \, , \qquad (3)$$

with J being the inertia of the tower-PMSG coupling, T_G being the generator electromagnetic torque and f being the viscous friction coefficient.

In Fig. 4, one can see the power and the torque characteristics *vs*. the rotational speed for a given value of the water flow velocity, both of which are unimodal, similar to the case of wind energy conversion systems [30] and marine current turbines [31]. This shows that the system model is non linear, the turbine torque being a nonlinear function of rotational speed and water flow velocity; hence a classical linear control structure requires model linearization around a steady-state operating point.

Based on Fig. 4, for a given water velocity value, supposed known and constant, and a given rotational speed value Ω_T the expression of torque T_T may be obtained by tangent linearization around the given operating point as a linear dependence of the rotational speed Ω_T:

$$T_T = T_{T0} + K \cdot \Omega_T \, , \qquad (4)$$

where T_{T0} is the torque at zero speed – supposed constant – and $K = \partial T_T / \partial \Omega_T$ is the mechanical characteristic's slope. One can note that slope K depends on the current operating point; moreover $K > 0$ for the ascending part of the torque curve and $K < 0$ for its descending part.

As briefly described before, the PMSG is vector-controlled by using the *dq* model frame, [8], [29]. By maintaining the direct-current component (i_{dG}) at zero (field oriented control), the PMSG torque is directly proportional with the quadrature (active) current (i_{qG}):

$$T_G = K_G \cdot i_{qG}\,, \tag{5}$$

where K_G is the torque constant. By replacing the expression of T_T and T_G given by (4) and (5) into (3) one obtains

$$J \cdot \dot{\Omega}_T - (K - f) \cdot \Omega_T = T_{T0} - K_G \cdot i_{qG}\,, \tag{6}$$

where notation $D = K - f$ can be used to denote a global parameter describing the combined effects of the torque characteristic slope and the friction coefficient.

By considering the variations around the steady-state operating point, the dynamic transfer from the current *q*-component, i_{qG}, to the tower rotational speed, Ω_T, can be characterized by the transfer function

$$H_\Omega(s) = \frac{\Omega_T(s)}{i_{qG}(s)} = -\frac{K_G}{Js - D}\,. \tag{7}$$

Open-loop transfer function (7) denotes a parameter-varying system because parameter *D* varies mainly due to the variability of the torque curve's slope *K* with the rotational speed (frictions being neglected). Further, recall that transfer function (7) has been obtained for a fixed value of the water velocity, whereas for other water velocity values both parameters *K* and *f* change. In conclusion, parameter $D = K - f$ varies with both the rotational speed and the water flow velocity. Another important remark is that – frictions being neglected – in the region corresponding to a positive slope, $K > 0$, the transfer function (7) is unstable. Also, note that the instability effect is more accentuated as the friction is smaller.

Instability of operating points placed on the ascending part of the torque curve can only be cancelled by control action, *i.e.*, in closed loop. Transfer function (7) suggests that the rotational speed can be controlled by a PI controller whose proportional gain determines the closed-loop system's stability. Thus, if the PI controller's transfer function is

$$H_C(s) = K_{p\Omega}\left(1 + 1/(T_{i\Omega} s)\right) \tag{8}$$

then the closed-loop transfer function becomes:

$$H_0(s) = \frac{T_{i\Omega} \cdot s + 1}{-\frac{JT_{i\Omega}}{K_G K_{p\Omega}} \cdot s^2 + T_{i\Omega}\left(\frac{D}{K_G K_{p\Omega}} + 1\right) \cdot s + 1} \tag{9}$$

Operating point change causes variation of parameter *D*. Equation (9) shows that the closed-loop bandwidth $\omega_0 = \sqrt{-K_{p\Omega} K_G / JT_{i\Omega}}$ does not depend on the operating point. This is not the case for its damping coefficient, which however varies slightly for a sufficiently high absolute value of loop gain, $K_{p\Omega}$. Algebraic stability criteria show that, in order for dynamical system (9) to be stable for any operating point, the gain $K_{p\Omega} < 0$ and moreover its absolute value should be sufficiently large:

$$\left|K_{p\Omega}\right| > D_{\max} / K_G\,, \tag{10}$$

where $D_{\max}$ corresponds to the maximum value of slope in the unstable region of the turbine torque characteristic, for all water flow velocities. Fig. 4 suggests that a typical operating point will be placed on the negative slope of the torque characteristic, *i.e.*, around the maximum power point. However, as the turbine blades are not pitchable, and the turbines are not allowed to operate in very high rotational speed range, the sole possibility of reducing the turbine captured power is to reduce its rotational speed and to force its operation in the unstable region – the so-called active stall control. Similar operating regime takes place while the system is started. So, the CFWT system should be able to operate in a broad range, covering most of the torque curve in Fig. 4.

Note that in practice, due to inherent delays, a too high value of $K_{p\Omega}$ can induce stability problems on the negative-slope region of the torque curve as the phase margin may become too small. Hence, value of $K_{p\Omega}$ should in practice be chosen as a trade-off between closed-loop performances desired in the two above-described operating regions. $K_{p\Omega}$ and $T_{i\Omega}$ are solutions of a second-order system of equations which results from imposing some desired settling time and overshoot in closed loop, *i.e.*, to transfer function (9) [32].

Note also that using this strategy for high water flow velocity values, where the power limitation is fully justified, leads to a strong increase of the generator and turbine torque. This appears to be a general phenomenon emphasized for stall-controlled fixed-pitch turbines immerged in any fluid (wind [33] or water [34]). As a consequence, generators should be torque over-rated, in order to allow such kind of operation (see data in the Appendix).

VII. Operation assessment of the CFWT-based generation system

A. Water flow properties and measurement system

This section presents some brief description of water flow properties, together with the measurement system used to quantify them. Their in-depth study is beyond the scope of this paper, but they are needed to understand the fluid-structure interactions and conditions of experimental results. An interested reader is referred to [24] and [35].

Related to homogeneity of water flow, the turbulence intensity I is defined as the ratio between the standard deviation of water flow velocity variations and the local averaged velocity. I depends of Reynolds number Re according to $I = 0.16 \cdot Re^{-0.125}$, where $Re = w_0 \cdot D/w$, with w_0 being the free-stream water flow velocity, D the turbine diameter and w the water flow velocity experienced by the turbine. Typically, for a free-flow tube in laboratory conditions, turbulence intensity is between 2 and 10%. Note that in our case w is significantly increased due to fairings, which results in a small Reynolds number, therefore turbulence intensity is expected to be reduced. Hence, for the experiments reported here one can reasonable assume conditions of turbulence less than 10%. Border effects can also reasonably be neglected because canal shores are placed at more than two meters from a side and the other of the CFWT system (see CFWT and fairings dimensions in the Appendix).

Water flow velocity is measured by means of two Doppler-effect-based transducers: the Acoustic Doppler Current Profiler (ADCP – mounted on a small trimaran ship) and an ARGONAUT SW transducer, installed 35 m upstream of the CFWT system, in order to account for the free-stream velocity. Supply and data cables connect this latter transducer to the energy supply and data logging system within the shelter. The ADCP allows to measure the components of water flow velocity on the three spatial coordinates. For quality sake, a homogeneity assumption about the velocity field is adopted at the level of this transducer; thus, if the three measures are too different, then the field is considered too disturbed and the measure is rejected, as considered false.

B. Stable vs. unstable operation

Fig. 5a presents a case of unstable operation of the CFWT-based system. During the first tests on the prototype, unstable operation is characterized by mechanical vibrations of the whole structure, which are reflected in oscillations of the mechanical variables, such as rotational speed and torque. In this figure the rotational speed reference is a slowly-variable ramp – first increasing and then decreasing – for both towers composing the system. These oscillations have been predicted by theoretical analysis detailed in Section V; they are due to operation on the ascending zone of the torque characteristic (Fig. 4), where transfer function (7) has unstable poles.

Rotational speed controller parameters must be computed so that the instability be cancelled in closed loop – in other words, the characteristic polynomial of transfer function (9) should be Hurwitz. Fig. 5a illustrates a case where controller proportional gain $K_{p\Omega}$ does not meet condition (10) in all operating range. Under the same test conditions as in Fig. 5a, Fig. 5b shows the results obtained by doubling the value of $K_{p\Omega}$, in which system operates without oscillations. Rated values in these figures are those of generators (*i.e.*, rated torque 468 Nm and rotational speed 330 rpm). Torque values are computed with (5), where i_{qG} is computed through Park transform based on generator's three-phase current measures.

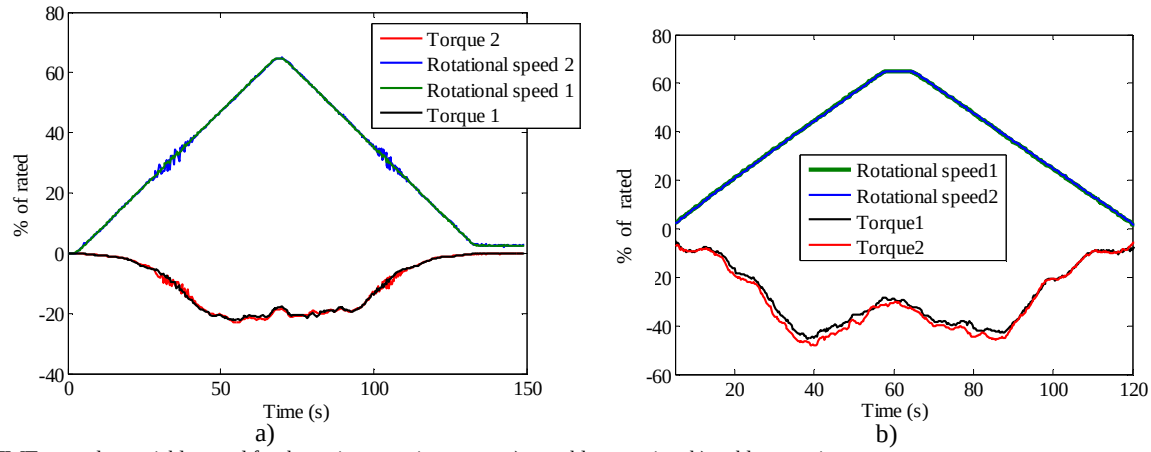

Fig. 5. CFWT control at variable speed for the entire operating range: a) unstable operation; b) stable operation.

These new controller parameters will be used for future tests; they are listed in the Appendix.

C. Steady-state characterization

Based on results shown in Fig. 5b, which were obtained for water velocity of about 1.9 m/s, it is possible to reach a steady-state operating point, hence to extract the various steady-state characteristics of CFWT towers. For sake of clarity, in this section power and torque evolutions are represented by positive values. Results in Fig. 6a show power *vs.* rotational speed steady-state characteristics, whereas those in Fig. 6b present torque *vs.* rotational speed steady-state characteristics, power values being

computed with (2) based on torque values previously obtained. Here also rated values are those of generators (*i.e.*, rated power 16.2 kW, rated torque 468 Nm and rotational speed 330 rpm). In both figures continuous thin lines correspond to measured points – smoothed by filtering – and dashed thick lines are identified by polynomial curve fitting. Polynomials representing power *vs.* rotational speed and torque *vs.* rotational speed dependences are given in (11) and (12), respectively.

Power characteristic has a maximum value (22% ± 2%) that corresponds to a large rotational speed range (60% ± 10%) – denoted by $\Delta\Omega$ in Fig. 6a – because of its flat shape around the maximum. The flat shape of this curve influences the convergence speed of MPPT algorithms [30], [36]. The experimentally-obtained characteristics from Fig. 6 are in good agreement with their theoretical counterparts – see [21] and Fig. 4. One can obtain from the maximum slope of the torque characteristic (traced for the rated water velocity value) the minimal proportional gain value, $K_{p\Omega}$, that stabilizes the system operation in the unstable region, according to (10).

$$y_P(x=\Omega) = -1.7^{-10}\cdot x^7 + 4.6\cdot 10^{-8}\cdot x^6 - 4.7\cdot 10^{-6}\cdot x^5 + 2.3\cdot 10^{-4}\cdot x^4 - 5.1\cdot 10^{-3}\cdot x^3 + 0.056\cdot x^2 - 0.18\cdot x + 0.12\,, \quad (11)$$

$$y_T(x=\Omega) = -2.10^{-10}\cdot x^7 + 4.7\cdot 10^{-8}\cdot x^6 - 3\cdot 9\cdot 10^{-6}\cdot x^5 + 1.1\cdot 10^{-4}\cdot x^4 + 8\cdot 10^{-5}\cdot x^3 - 0.032\cdot x^2 + 0.52\cdot x + 2.5\,, \quad (12)$$

$$y_{Cp}(x=\lambda) = -0.018\cdot x^7 + 0.23\cdot x^6 - 1.1\cdot x^5 + 2.3\cdot x^4 - 2.4\cdot x^3 + 1.2\cdot x^2 - 0.17\cdot x + 0.005\,. \quad (13)$$

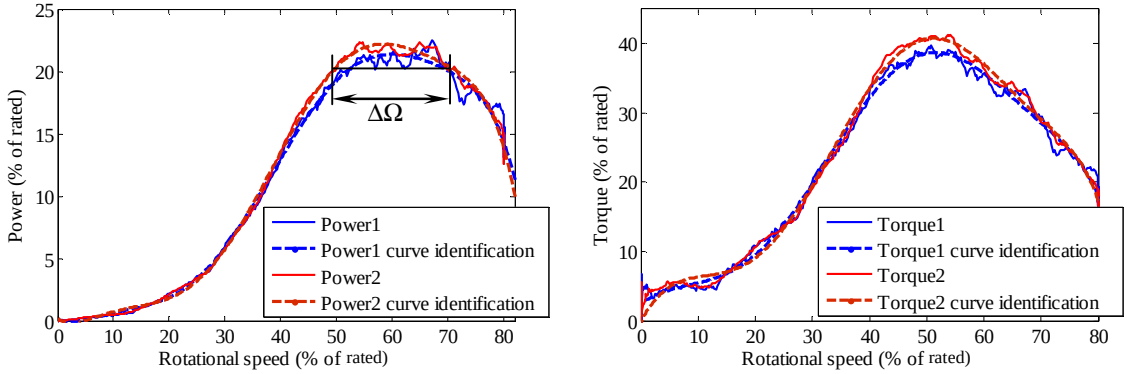

a) b)

Fig. 6. Steady-state characteristics for both CFWT systems: a) power *vs.* rotational speed curves, b) torque *vs.* rotational speed curves.

Other information as start-up torque, maximum torque, maximum power point value, *etc.*, for a certain water velocity may also be extracted from the identified curves.

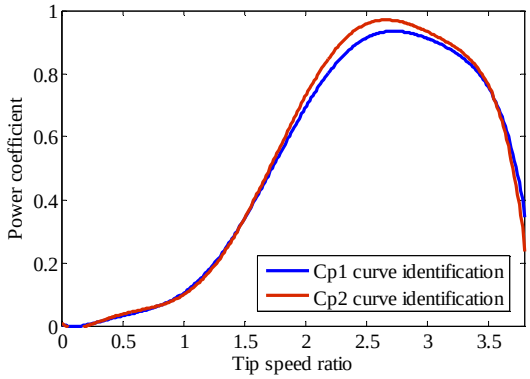

Fig. 7. Power coefficient as function of the tip-speed ratio.

By using torque measured values and taking into account the turbine geometry, the dependence of the power coefficient on the tip speed ratio is also identified, by combining relations (1) and (2), as shown in Fig. 7. This figure allows the assessment of the maximum yield of the power take-off device and the associated operating conditions: the maximum value of the power coefficient C_{p_max}, as well as the corresponding tip speed ratio. The curve-fitting polynomial representing torque *vs.* rotational speed is given by (13), which can further be used in system modeling and simulations in various scenarios in order to predict system performance.

Note that the power characteristic curve has been obtained by using (1), which gives the captured power in free-fluid conditions. That is, *w* in (1) represents the free-stream water flow velocity, whereas the velocity effectively experienced by the turbines is significantly increased due to fairings (see Section VII.A). Thus, formally speaking, (1) is no longer valid, and the captured power value is larger than predicted. However, by using a conceptual abuse, one may state that this corresponds to an

increase in the power coefficient value, if computed by using the same equation as in the free-flow conditions. This explains the unusually large value of the power coefficient C_p (much larger than results predicted by Betz's theory [37]). Note that C_p evaluation while taking into account that fairings increase the projected cross-flow surface would give results coherent with Betz' theory. So, for the studied system, λ_{opt} is approximately 2.5 and C_{p_max} is close to 1. This is coherent with the results in [24], where the global C_p averaged on a complete rotation of an Achard turbine without fairings is reported to be 0.49 at optimal $\lambda = 1.8$, whereas with fairings C_p reaches 1.272 for optimal $\lambda = 2.5$.

D. Maximum power point tracking (MPPT)

Here, a gradient-based method of maximum power point tracking (MPPT) was implemented for a single tower, where the rotational speed reference is updated every T_s seconds by:

$$\Omega_k = \Omega_{k-1} + \int_{t_{k-1}}^{t_k} K_{MPPT} \cdot \mathrm{sgn}\left(P_k - P_{k-1}\right) \cdot \mathrm{sgn}\left(\Omega_k - \Omega_{k-1}\right), \qquad (14)$$

where index k denotes successive discrete time points such that $T_s = t_k - t_{k-1}$, with Ω_k and P_k being rotational speed and power values at time t_k, respectively, and coefficient K_{MPPT} being responsible for the convergence speed. Measured values of rotational speed and power – computed as the product of rotational speed by torque – were low-pass filtered with a time constant of 1 s in order to eliminate high-frequency noise. This time constant must be taken into account in setting the value of T_s, which, for its part, influences choice of K_{MPPT}. Fig. 8 presents results obtained when both generators operate at MPPT independently under almost constant water velocity, where the rated rotational speed is that of the generators (*i.e.*, 330 rpm). For this test, the convergence speed parameter was chosen $K_{MPPT} = 1$. It clearly appears that the MPPT convergence speed is good. However, value of K_{MPPT} should ideally be decreased as system approaches the MPP.

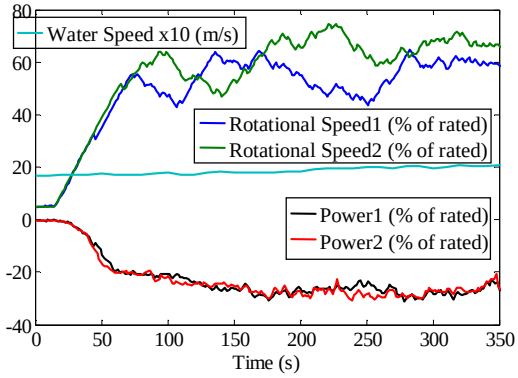

Fig. 8. Evolution of main variables when both towers are operated at MPPT.

This figure also shows that, in order to reach the maximum power on both generators (the two maximum power values are typically very close), the MPPT controller imposes different speed references: the rotational speed of the first tower is increased, whereas for the second one it is decreased. This is due to multiple reasons, one of which may be that towers shadows each other, hence each of them is placed in the wake of the other. In-depth study of these aspects is a point of future research. Second, their power and torque characteristics are not precisely the same because of differences between hydrodynamic characteristics of the two towers. The real maximum power point is slightly offset on each tower in relation to the theoretical maximum power point. Another reason is the flat shape of the power curve around its maximum. So approximately the same power value (close to maximum) is obtained for a large variation range of rotational speed (see also Fig. 6a). As mentioned above, adaptive versions of MPPT – where gain K_{MPPT} is made variable depending on the distance from MPP – may be employed in order to determine more precisely the MPP rotational speed.

E. Synchronization between the two towers

The system is composed of two independent towers which can be synchronized in both speed and position, whenever the application would require such synchronization; real-time validations of control results for this case are reported in [22]. Synchronization supposes that rotational speeds of towers are equal, but also their positions (orientation angles in relation with same reference position). Such synchronization may be necessary for reducing mechanical loads and also turbulence intensity due to the wake effect [24]. It is possible to synchronize the two towers by using the master-slave principle: the slave tower will follow the actual speed and actual position of the master tower. It is also possible to keep positions of the two towers shifted by a nonzero angle offset.

Fig. 9 shows how the position error – defined as the difference between positions of the two towers – evolves when the angle offset reference is set to zero and master's rotational speed increases as a slowly-variable ramp. Fig. 10 shows evolution in

response to a step change of angle offset reference from zero to π. The position error is close to zero and the two rotational speeds are only slightly impacted. During normal operation, the offset angle may suffer variations less abrupt than a step, which means that the impact on main variables is even slighter.

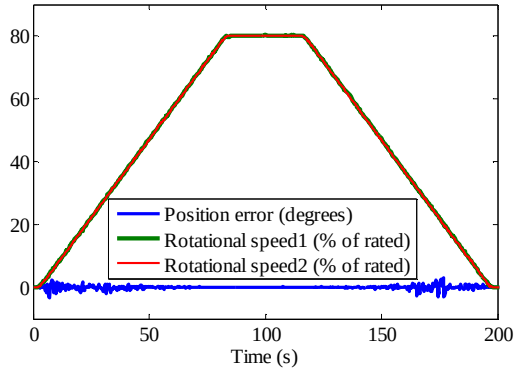

Fig. 9. Rotational speeds and position error of towers when these are synchronized according to the master-slave principle.

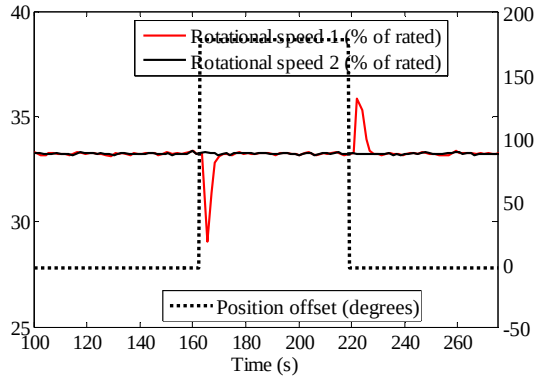

Fig. 10. Illustration of response to step change of angle offset in synchronized operation.

F. Synchronization with MPPT

This section discusses results when the two towers are synchronized and the master tower is operated at MPPT. Note that, when the system is in MPPT mode, the speed reference is continuously updated, which renders the synchronization more challenging than in other cases. It is reasonable to consider that the angle offset does not normally vary step-like or too fast. A continuous triangle variation of the angle offset reference is applied to validate the synchronization loop with MPPT. The result of this test is shown in Fig. 11.

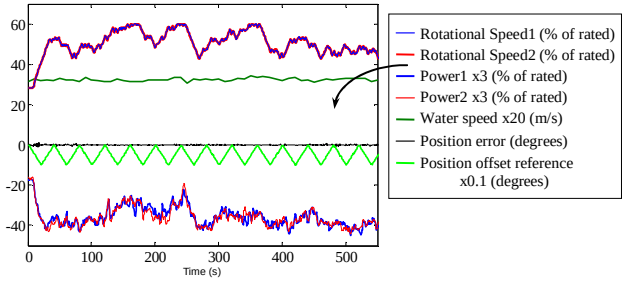

Fig. 11. Time evolutions of main variables when the two towers are synchronized and the master tower is in MPPT.

The MPPT allows the system to track changes in the water velocity, which is reflected in rotational speed variations. The position error is corrected to zero despite the continuous variation of the angle offset reference. These results are perfectly coherent with real-time simulations results in [22].

VIII. Conclusion

This paper reported on the basic operation assessment of electrical power generation using a system based on cross-flow water turbines. The specific power take-off system is composed of two towers – each of which is composed of four piled-up cross-flow water turbines – which rotate in opposite senses. Fairings have been added to the resulted generation system in order to increase its global efficiency. A 1:1 prototype was built based on industrial equipment, in order to allow electrical power conversion tests in a real-world setup.

Real-world results confirm preliminary conclusion concerning both steady-state and dynamical characteristics, as issued from previous modeling assessments and simulations. These results illustrate power generation chain operation and allow global efficiency estimation of the CFWT-based prototype system. System mechanical characteristics – torque *vs*. rotational speed and power vs rotational speed – as well as power coefficient curve were traced; they confirm simulation results previously obtained. Certain elements regarding dynamical behavior of CFWT-based system – e.g., movement equation – were also validated.

IX. Appendix

CFWT system data: Radius R = 0.25 m, Height of a single turbine = 0.5 m, Output rated power 16 kW at water flow velocity 2.8 m/s, Maximum power coefficient C_{p_max} = 0.95, optimal tip speed ratio λ_{opt} = 2.7.

Canal: width = 8 m, depth = 4 m, rated flow rate = 70 m^3/s for water velocity at 2.2 m/s.

Fairings: Profile EPPLER-420, Chord length = 1 m, Incidence angle (angle of attack) = 15° (see Fig. 12).

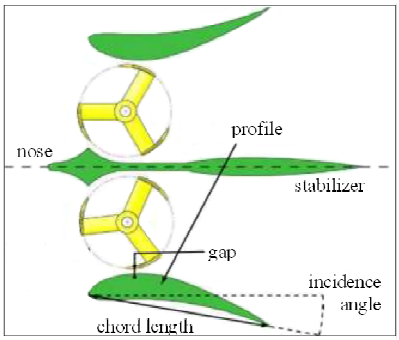

Fig. 12. Transversal view of the two towers and their fairings [24], [35].

PMSG and electric specifications: Rated power 16.2 kW, Rated rotational speed 330 rpm, Rated torque 468 Nm; Dump load 34.1 Ω, Dump load power 15 kW, DC-link voltage 690 V.

Measurement system: Doppler-effect-based fixed acoustic transducer (Sontek ARGONAUT SW) for water velocity between 0.3 m/s and 5 m/s; on-generator-shaft encoders/resolvers for turbines' rotational speed; three-phase generator current transducers.

Control specifications: *dq* current PI controller: Proportional gain 30, Integral gain 15 s^{-1}; Rotational speed PI controller: Proportional gain 60, Integral time constant 100ms; MPPT parameters: T_s = 5 s, K_{MPPT} = 0.25 ÷ 1.

X. References

[1] M. J. Khan, G. Bhuyan, M. T. Iqbal, and J. E. Quaicoe, "Hydrokinetic energy conversion systems and assessment of horizontal and vertical axis turbines for river and tidal applications: A technology status review," *Applied Energy*, vol. 86, pp. 1823-1835, 2009.

[2] M. Benbouzid, J. A. Astolfi, S. Bacha, J. F. Charpentier, M. Machmoum, T. Maître, and D. Roye, "Concepts, modeling and control of tidal turbines," in: *Marine Renewable Energy Handbook*, pp. 219-278, 2013.

[3] Z. Zhou, M. Benbouzid, J. F. Charpentier, F. Scuiller, and T. Tang, "Developments in large marine current turbine technologies–A review," *Renewable and Sustainable Energy Reviews*, vol. 71, pp. 852-858, 2017.

[4] F. Hernández, L. E. Chiang, P. Corbalán, "A general architecture for electric power management of small scale NCRE converters: Design methodology and validation," *Energy for Sustainable Development*, vol. 41, pp. 128–138, 2017.

[5] H. H. H. Aly, "Dynamic modeling and control of the tidal current turbine using DFIG and DDPMSG for power system stability analysis," *Electrical Power and Energy Systems*, vol. 83, pp. 525–540, 2016.

[6] S. Mehri, M. Shafie-khah, P. Siano, M. Moallem, M. Mokhtari, and J.P.S. Catalão, "Contribution of tidal power generation system for damping inter-area oscillation," *Energy Conversion and Management*, vol. 132, pp. 136–146, 2017.

[7] B. Whitby. and C. E. Ugalde-Loo, "Performance of pitch and stall regulated tidal stream turbines, " *IEEE Trans. on Sustainable Energy*, vol. 5, no. 1, pp.64-72, 2014.

[8] Z. Zhou, F. Scuiller, J. F. Charpentier, M. E. H. Benbouzid, and T. Tang, "Power smoothing control in a grid-connected marine current turbine system for compensating swell effect," *IEEE Trans. on Sustainable Energy*, vol. 4, no. 3, pp.816-826, 2013.

[9] K. Golecha, T. I. Eldho, and S. V. Prabhu, "Influence of the deflector plate on the performance of modified Savonius water turbine," *Applied Energy*, vol. 88, pp. 3207-3217, 2011.
[10] S. Lundin, J. Forslund, A. Goude, M. Grabbe, K. Yuen, and M. Leijon, "Experimental demonstration of performance of a vertical axis marine current turbine in a river," *Journal of Renewable and Sustainable Energy*, vol. 8, no. 6, 2016, DOI: http://dx.doi.org/10.1063/1.4971817.
[11] M. Shiono, K. Suzuki, and S. Kiho, "An experimental study of the characteristics of a Darrieus turbine for tidal power generation," *Electrical Engineering in Japan*, vol. 132, no. 3, pp. 38-47, 2000.
[12] J.-L. Achard, and T. Maître (Grenoble Institute of Technology). Hydraulic turbomachine, European Patent EP 1718863, 2008.
[13] S. B. Elghali, M. E. H. Benbouzid, and J. F. Charpentier, "Modelling and control of a marine current turbine-driven doubly fed induction generator," *IET Renewable Power Generation*, vol. 4, no. 1, pp. 1-11, 2010.
[14] L. Myers, and A. S. Bahaj, "Wake studies of a 1/30th scale horizontal axis marine current turbine," *Ocean Engineering*, vol. 34, pp. 758-762, 2007.
[15] J-H. Chen, F.-C. Chiu, C.-Y. Hsin, and J.-F. Tsai, "Hydrodynamic consideration in ocean current turbine design," *Journal of Hydrodynamics*, vol. 28, no. 6, pp. 1037-1042, 2016.
[16] A. N. Gorban, A. M. Gorlov, and V. M. Silantyev, "Limits of the turbine efficiency for free fluid flow," *Journal of Energy Resources Technology*, vol. 123, pp. 311-317, 2001.
[17] S. Antheaume, T. Maître, and J.-L. Achard, "Hydraulic Darrieus turbines efficiency for free fluid flow conditions versus power farms conditions," *Renewable Energy*, vol. 33, pp. 2186-2198, 2008.
[18] I. Loots, M. van Dijk, B. Barta, S. J. van Vuuren, and J. N. Bhagwan, "A review of low head hydropower technologies and applications in a South African context," *Renewable and Sustainable Energy Reviews*, vol. 50, pp. 1254–1268, 2015.
[19] D. Kumar, and S. Sarkar, "A review on the technology, performance, design optimization, reliability, techno-economics and environmental impacts of hydrokinetic energy conversion systems," *Renewable and Sustainable Energy Reviews*, vol. 58, pp. 796–813, 2016.
[20] F. Behrouzi, M. Nakisa, A. Maimun, and Y. M. Ahmed "Global renewable energy and its potential in Malaysia: A review of hydrokinetic turbine technology," *Renewable and Sustainable Energy Reviews*, vol. 62, pp. 1270–1281, 2016.
[21] M. Andreica, *Energy optimization of micro-hydro-electrical conversion chains – modelling, control and experimental tests* (in French: *Optimisation énergétique de chaînes de conversion hydroliennes – modélisations, commandes et réalisations expérimentales*). Ph.D. Thesis, Grenoble Institute of Technology, 2009.
[22] M. Vallet, I. Munteanu, A.I. Bratcu, S. Bacha, and D. Roye, "Synchronized Control Of Cross-Flow-Water-Turbine-Based Twin Towers," *Renewable Energy*, vol. 48, pp. 382-391, 2012.
[23] M. Hauck, A. Rumeau, I. Munteanu, A.I. Bratcu, S. Bacha, D. Roye, and A. Hably, "A 1:1 prototype of power generation system based upon cross-flow water turbines," in *Procs. of 2012 IEEE International Symposium on Industrial Electronics* – ISIE 2012, pp. 1414-1418, 2012.
[24] T. Jaquier, *Cross-flow water turbines: development of a prototype in river canal* (in French: *Hydroliennes à flux transverse : développement d'un prototype HARVEST en canal*). Ph.D. Thesis, Grenoble Institute of Technology, 2011.
[25] V. Aumelas, and T. Maître, "Development of an experimental facility for cross flow water turbine models," in *Procs. of the 4th International Conference on Energy and Environment*, Bucharest, Romania, November 12-14 2009.
[26] ***, Parker permanent-magnet synchronous motors data sheet: http://www.parker.com/portal/site/PARKER/menuitem.de7b26ee6a659c147cf26710237ad1ca/?vgnextoid=fcc9b5bbec622110VgnVCM10000032a71dacRCRD&vgnextcatid=7857700&vgnextcat=TKW+FRAMELESS+TORQUE+MOTORS&vgnextfmt=EN. Available June 2017.
[27] ***, Parker modular system AC drive data sheet: http://www.parker.com/portal/site/PARKER/menuitem.338f315e827b2c6315731910237ad1ca/?vgnextoid=093c1eee6b5ae210VgnVCM10000048021dacRCRD&vgnextfmt=EN&vgnextfmt=EN&productcategory=partlist&vgnextdiv=688297&vgnextcatid=11804750&vgnextcat=AC890+MODULAR+SYSTEM+AC+DRIVE&Wtky=. Available June 2017.
[28] ***, SDMO internal combustion motor and synchronous electrical generator data sheet: http://www.sdmo.com/EN. Available June 2017.
[29] B. K. Bose, *Modern Power Electronics and AC Drives*. Englewood Cliffs: Prentice – Hall, 2001.
[30] I. Munteanu, A. I. Bratcu, N.-A. Cutululis, and E. Ceangă, *Optimal Control of Wind Energy Systems – Towards a Global Approach*. London: Springer-Verlag, 2008.
[31] S. Ben Elghali, M. Benbouzid, J. Charpentier, T. Ahmed-Ali, and I. Munteanu, "Experimental Validation of a Marine Current Turbine Simulator: Application to a PMSG-Based System Second-Order Sliding Mode Control," *IEEE Trans. on Industrial Electronics*, vol. 58, no. 1, pp. 118-126, 2011.
[32] K. Åström, and T. Hägglund, "PID Control," in *The Control Handbook* (Ed. W. S. Levine), pp. 198-209. CRC Press, 1996.
[33] A. Burlibașa, I. Munteanu, and A.I. Bratcu, "Unitary power control strategy for low-power wind energy conversion system using active speed stall control for full-load regime," *IET Renewable Power Generation*, vol. 8, no. 6, pp. 696-706, 2014.
[34] M. Arnold, F. Biskup, and P.W. Cheng, "Load Reduction Potential of Variable Speed Control Approaches for Fixed Pitch Tidal Current Turbines," in *Procs. of the 11th European Wave and Tidal Energy Conference* – EWTEC 2015, Nantes, France, September 6-11 2015.
[35] A. Duval, E. Châtelet, G. Jacquet, J. Zanette, T. Jaquier, and T. Maître, "Fluid/structure interaction and dynamic response of vertical axis water turbines," in *Procs. of the 17th Symposium on Vibrations, Shocks and Noise*, Lyon, France, June 15-17 2010.
[36] M. Hauck, I. Munteanu, A.I. Bratcu, S. Bacha, and D. Roye, "Operation of Grid-Connected Cross-Flow Water Turbines in the Stall Region by Direct Power Control," *IEEE Trans. on Industrial Electronics*, vol. 58, no. 4, pp. 1132-1140, 2011.
[37] A. Betz, *Wind energy and its use by wind-mills* (in German: *Wind-Energie und ihre Ausnutzung durch Windmühlen*). Göttingen: Vandenhoek & Ruprecht, 1926.